PHILOSOPHICAL TRANSACTIONS A

royalsocietypublishing.org/journal/rsta

Research

Cite this article: Kolinichenko AP, Pisarchik AN, Ryashko LB. 2020 Stochastic phenomena in pattern formation for distributed nonlinear systems. *Phil. Trans. R. Soc. A* **378**: 20190252. http://dx.doi.org/10.1098/rsta.2019.0252

Accepted: 6 November 2019

One contribution of 18 to a theme issue 'Patterns in soft and biological matters'.

Subject Areas:
computational biology, computer modelling and simulation, biomathematics, chaos theory, statistical physics, mathematical modelling

Keywords:
self-organization, Turing instability, population dynamics, noise

Author for correspondence:
A. N. Pisarchik
e-mail: alexander.pisarchik@ctb.upm.es

THE ROYAL SOCIETY PUBLISHING

Stochastic phenomena in pattern formation for distributed nonlinear systems

A. P. Kolinichenko[1], A. N. Pisarchik[2] and L. B. Ryashko[1]

[1]Ural Federal University, Ekaterinburg, Russia
[2]Centre for Biomedical Technology, Technical University of Madrid, Madrid, Spain

ANP, 0000-0003-2471-2507; LR, 0000-0002-0817-3753

We study a stochastic spatially extended population model with diffusion, where we find the coexistence of multiple non-homogeneous spatial structures in the areas of Turing instability. Transient processes of pattern generation are studied in detail. We also investigate the influence of random perturbations on the pattern formation. Scenarios of noise-induced pattern generation and stochastic transformations are studied using numerical simulations and modality analysis.

This article is part of the theme issue 'Patterns in soft and biological matters'.

1. Introduction

Self-organization of matter has attracted the attention of researchers from various areas for many years. Diverse phenomena related to self-organization are encountered in physics, chemistry, biology, ecology and other fields of science [1–5]. However, the recreation of self-organization in laboratory conditions for the experimental study of underlying mechanisms is very complicated and extremely expensive. Consequently, the main research tools and techniques are mathematical modelling and the development of computational methods [6–8].

Long ago, Alan Turing suggested the phenomenon of diffusion instability (or Turing instability) [9,10] as one of the possible mechanisms of self-organization in nature. Among numerous papers devoted to modelling pattern formation in nature, we have to mention the animal coat pigmentation [11], population dynamics [12–14] and neuronal models [15]. It should be noted that significant efforts are being directed towards the creation of a comprehensive theory that would allow predicting and simulating processes which lead to self-organization.

Special attention was paid to studying the Turing bifurcation near the Andronov–Hopf bifurcation boundary [16–19]. In particular, it was shown that diffusion can transform homogeneous oscillatory modes into heterogeneous oscillations or suppress them entirely to form a stationary pattern. To simulate self-organization processes as best as possible, one has to take into account the effect of random perturbations in a dynamical system, where the interplay between nonlinearity and stochasticity can cause many unexpected phenomena [20–24]. Among them, we should mention noise-induced phase transitions [25–29] and stochastically forced self-organization [13,30,31]. Despite the fact that noise is caused by random processes, it often helps to establish a relative order in dynamical systems. Since respective models for studying self-organization are nonlinear and stochastic, analytical approaches are quite limited; therefore, asymptotic computational methods should be used [32].

In the present paper, we study the nonlinear predator–prey dynamical model [33,34]. We show that adding diffusion in this originally monostable system induces multiple coexisting spatial structures, thus resulting in multistability. In §2, we analyse the deterministic spatially distributed predator–prey population model within the Turing instability zone, where pattern formation is possible. The multistable behaviour is demonstrated with examples of various stable spatial heterogeneous structures. In addition, the peculiarities of temporal dynamics of pattern generation are analysed by the waveform pattern modality. Section 3 is devoted to stochastic phenomena, namely, noise-induced transitions between coexisting patterns in the Turing instability zone, and noise-induced pattern generation in the Turing stability zone. The modality analysis helps a lot in direct modelling. We demonstrate that even very weak noise affects particular modes and causes generation of specific patterns. Furthermore, the statistical analysis shows that the system may go through some kind of stochastic resonance where the patterns are more accented at a particular value of the noise intensity. Finally, the main conclusions are given in §4.

2. Multistability and transient processes in the deterministic model

We consider a spatially extended variant of the predator–prey population model [33,34] written as follows:

$$\left.\begin{aligned}\frac{\partial u}{\partial t} &= u(1-u) - v\sqrt{u} + D\frac{\partial^2 u}{\partial x^2}\\ \text{and}\qquad \frac{\partial v}{\partial t} &= cv\sqrt{u} - sv^2 + \frac{\partial^2 v}{\partial x^2}.\end{aligned}\right\} \tag{2.1}$$

Here, u and v are the densities of predator and prey populations; the predator consumes the prey with conversion intensity rate c. The mortality for both prey and predator is quadratic, which means internal competition of species. The parameter s shows the severity of the inner competition of predators as compared to prey.

The following zero-flux boundary conditions are assumed:

$$\left.\begin{aligned}\frac{\partial u}{\partial x}(t,0) &= \frac{\partial u}{\partial x}(t,L) = 0\\ \text{and}\qquad \frac{\partial v}{\partial x}(t,0) &= \frac{\partial v}{\partial x}(t,L) = 0.\end{aligned}\right\} \tag{2.2}$$

The meaning of these conditions is that the species do not arrive or escape through borders of a bounded space. In our model, the spatial variable x varies within the interval $[0, L]$ which represents the bounded space.

The non-extended model has a non-trivial equilibrium at $(\bar{u}, \bar{v}) = \left((s-c)/s, (c\sqrt{s-c})/\sqrt{s^3}\right)$. For $c = 1$, this equilibrium is stable for $s > s^* = 1.125$. Correspondingly, the distributed model (2.1) has a homogeneous equilibrium at $u(t,x) \equiv \bar{u}$, $v(t,x) \equiv \bar{v}$. Because of diffusion, this equilibrium

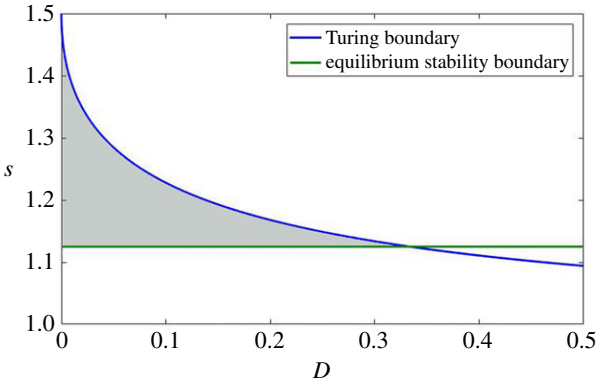

Figure 1. Bifurcation diagram of the distributed population model (2.1) with $c = 1$. (Online version in colour.)

is stable in the system (2.1), (2.2) for $D < D_*$, where the Turing bifurcation value D_* satisfies the following equation:

$$\left(\frac{3c-2s}{2s} - Dc\sqrt{\frac{s-c}{s}}\right)^2 - 4Dc\frac{1-3c+2s}{2s}\sqrt{\frac{s-c}{s}} = 0. \tag{2.3}$$

Hereinafter we fix $c = 1$ and study the system dynamics with respect to control parameters s and D.

Figure 1 shows the bifurcation diagram with $s = s_*$ (green line) and the Turing boundary $D = D_*$ (blue curve). The shaded area indicates the Turing instability zone where the non-homogeneous stable structures (patterns) are observed.

In this study, we perform numerical simulations using the following difference scheme:

$$\left.\begin{aligned} u_{j+1,i} &= u_{j,i} + \tau f_{j,i} + \tau D_u \frac{u_{j,i-1} - 2u_{j,i} + u_{j,i+1}}{h^2} \\ \text{and} \quad v_{j+1,i} &= v_{j,i} + \tau g_{j,i} + \tau D_v \frac{v_{j,i-1} - 2v_{j,i} + v_{j,i+1}}{h^2}, \end{aligned}\right\} \tag{2.4}$$

where

$$\begin{gathered} f_{j,i} = f(u_{j,i}, v_{j,i}), \quad g_{j,i} = g(u_{j,i}, v_{j,i}), \\ f(u,v) = u(1-u) - v\sqrt{u}, \quad g(u,v) = cv\sqrt{u} - sv^2, \\ u_{j,i} = u(t_j, x_i), \quad v_{j,i} = v(t_j, x_i), \ t_j = \tau j, \ x_i = hi, \\ \tau = 0.0001, \quad h = 0.2, \ L = 40, \ D_u = D, \ D_v = 1. \end{gathered}$$

The boundary conditions (2.2) are approximated as follows:

$$u_{j,0} = u_{j,1}, \quad v_{j,0} = v_{j,1}, \ u_{j,n} = u_{j,n-1}, \ v_{j,n} = v_{j,n-1} \quad \text{and} \quad L = nh.$$

In the numerical analysis, we use non-homogeneous initial conditions in the wave form

$$u_{0,i} = \bar{u} + \varepsilon \cos\left(\frac{2\pi\lambda ih}{L}\right), \quad v_{0,i} = \bar{v} + \varepsilon \cos\left(\frac{2\pi\lambda ih}{L}\right), \ i \in [0, n].$$

The parameter $\varepsilon \in [0, 0.1]$ characterizes the deviation of the initial wave from the homogeneous equilibrium and $\lambda \in [0, 12]$ is assumed to be integer or half-integer to satisfy the Neumann boundary conditions (2.2). The simulations are performed for different values of the diffusion coefficient D and fixed $s = 1.2$.

The generated patterns emerge as wave-like structures with different numbers of peaks and different shapes (ascending ↑ or descending ↓) near $x = 0$. These waves can be interpreted as areas

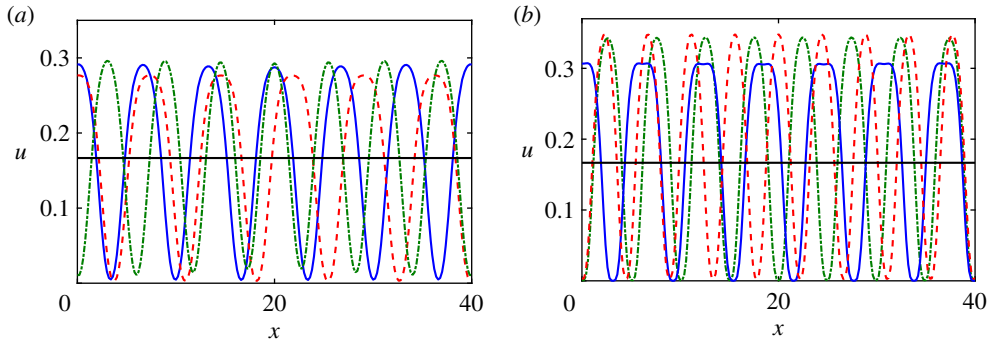

Figure 2. Examples of patterns in the system (2.1), (2.2) with $s = 1.2$ and $c = 1$ for (*a*) $D = 0.1$ and (*b*) $D = 0.05$. The horizontal lines stand for a homogeneous equilibrium state. (Online version in colour.)

of higher and lower population densities. Typical examples of these structures are illustrated in figure 2.

In figure 2*a*, we plot three different pattern-attractors obtained at the fixed parameters $s = 1.2$, $c = 1$ and $D = 0.1$ for different values of ε and λ. The solid blue curve shows the waveform of $u(x)$ for $\varepsilon = 0.1$ and $\lambda = 4$. It contains six complete periods and six peaks. When x is increased from $x = 0$, this wave descends. We mark this pattern as $(6\downarrow)$. Next, the dashed red wave contains 5.5 periods starting with a descending region, and therefore we mark this pattern as $(5.5\downarrow)$. This is the example of a half-integer pattern which was obtained for $\varepsilon = 0.1$ and $\lambda = 5.5$. Finally, the dotted green wave represents a $(7\uparrow)$ pattern formed for $\varepsilon = 0.05$ and $\lambda = 8$. Figure 2*b* shows other examples of the patterns generated for $D = 0.05$. The solid blue wave $(6.5\downarrow)$ is obtained for $\varepsilon = 0.05$ and $\lambda = 6.5$, the dashed red wave for $(9\uparrow)$ for $\varepsilon = 0.1$ and $\lambda = 4.5$ and the dotted green wave $(8\uparrow)$ for $\varepsilon = 0.05$ and $\lambda = 12$.

To summarize, the deterministic model (2.1), (2.2) exhibits a multistable behaviour with diverse patterns. For any fixed set of the system parameters, one can obtain different patterns corresponding to various initial conditions.

Temporal dynamics of the pattern formation is another important issue. Now, we will visualize the transient process by snapshots at different times and colour diagrams. Figure 3 demonstrates the evolution process for $s = 1.2$, $c = 1$, $D = 1$, $\lambda = 6$ and $\varepsilon = 0.01$. Here, the solid horizontal line stands for the homogeneous equilibrium state. In figure 3*e*, we present the complete transient process. Here, the abscissa is the time, the ordinate is the spatial variable x, and the colour indicates the population density of the prey. One can see that the transition from the initial $(2\downarrow)$-wave to the final $(8\uparrow)$-pattern is complex and multistage.

Another example of the complex multistage transition is illustrated in figure 4, where we show the pattern evolution from initial $(12\downarrow)$ wave to the final $(8\uparrow)$ attractor for $\varepsilon = 0.1$ and $\lambda = 12$. In the transition process, the transient pattern-attractors $(11\uparrow)$ and $(9\uparrow)$ occur.

For a quantitative description of qualitative changes in pattern formation, we carry out the modality analysis by considering the following modality coefficients:

$$C_k(t) = \int_0^L u(t,x)\cos\left(\frac{2\pi xk}{L}\right)\mathrm{d}x, \tag{2.5}$$

where each k corresponds to the number of pattern peaks, that can be either integer or half-integer due to Neumann boundary conditions. The structure with the highest absolute value of C_k is called *dominant*, and it is the most prominent structure at this moment. Figure 5 illustrates the application of this method to the transient process of pattern formation illustrated in figure 4.

Note that at the beginning of the simulation, the coefficient C_{12} dominates, so that a 12-peak pattern is observed. Later, this value decreases, while C_{11} grows and becomes dominant. Finally, all C_k begin to tend to zero with only C_8 remaining dominant.

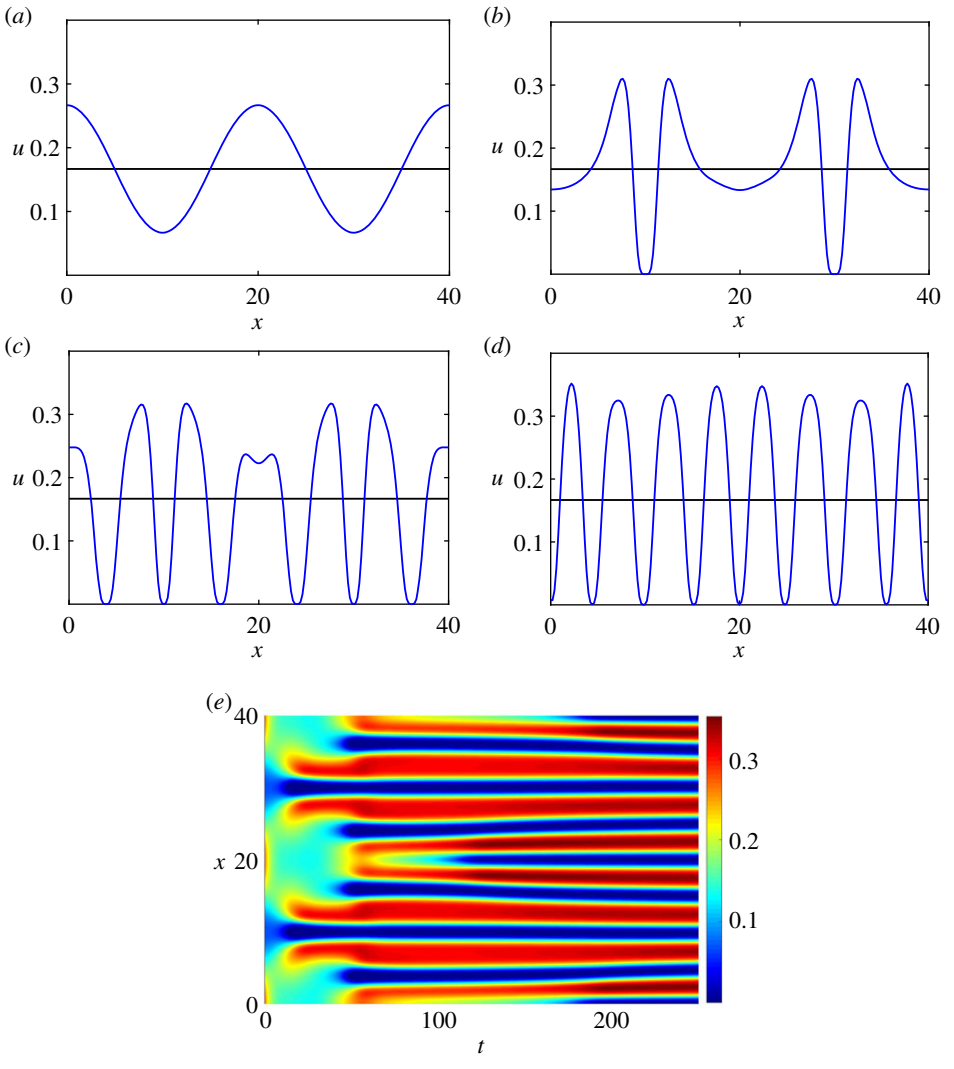

Figure 3. Pattern formation in the system (2.1), (2.2) for $s = 1.2$, $c = 1$, $D = 0.05$, $\varepsilon = 0.1$, $\lambda = 2$ and (*a*) $t = 0$, (*b*) $t = 25$, (*c*) $t = 50$, (*d*) $t = 200$ and (*e*) colour diagram of the transient process. (Online version in colour.)

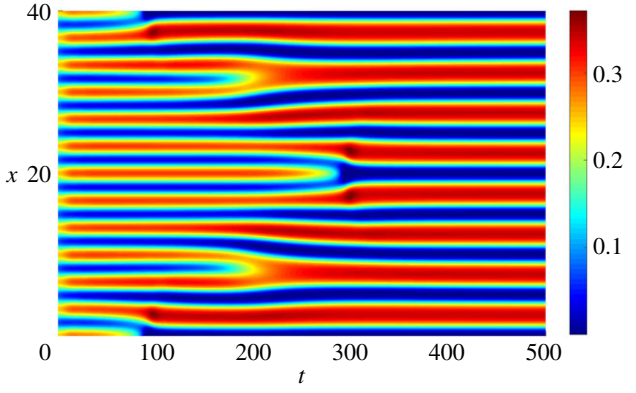

Figure 4. Pattern transition dynamics for $s = 1.2$, $c = 1$, $D = 0.05$, $\varepsilon = 0.1$ and $\lambda = 12$. (Online version in colour.)

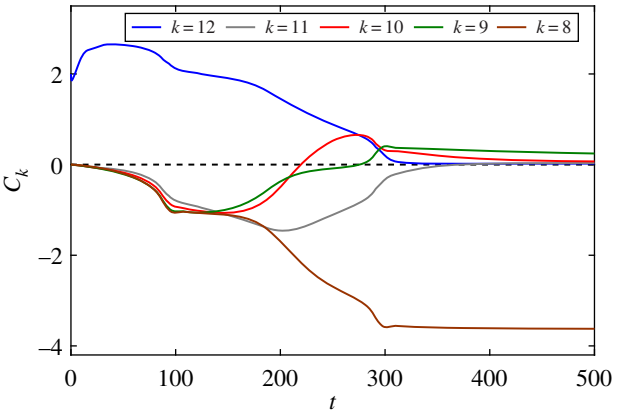

Figure 5. Modality analysis of transient patterns in the system (2.1), (2.2) with $s = 1.2$, $c = 1$, $D = 0.05$, $\varepsilon = 0.1$ and $\lambda = 12$. (Online version in colour.)

Thus, this modality method allows us to quantify the complex system evolution process.

3. Noise-induced phenomena in the stochastic model

In order to study the stochastic phenomena, we use the following model with random perturbations:

$$\left.\begin{aligned} \frac{\partial u}{\partial t} &= u(1-u) - v\sqrt{u} + D\frac{\partial^2 u}{\partial x^2} + \gamma_1 \xi(t,x) \\ \text{and} \quad \frac{\partial v}{\partial t} &= cv\sqrt{u} - sv^2 + \frac{\partial^2 v}{\partial x^2} + \gamma_2 \eta(t,x) \end{aligned}\right\} \tag{3.1}$$

and the same boundary condition (2.2). Here, $\xi(t,x)$ and $\eta(t,x)$ are uncorrelated Gaussian noises with intensities γ_1, γ_2 and parameters $\langle \xi(t,x)\rangle = \langle \eta(t,x)\rangle = 0$, $\langle \xi(t,x)\xi(s,y)\rangle = \delta(s-t)\delta(y-x)$, $\langle \eta(t,x)\eta(s,y)\rangle = \delta(s-t)\delta(y-x)$. In what follows, we assume $\gamma_1 = \gamma_2 = \gamma$.

In our computer simulations of the system (3.1), (2.2), we use the following stochastic numerical scheme:

$$\left.\begin{aligned} u_{j+1,i} &= u_{j,i} + \tau f_{j,i} + \tau D_u \frac{u_{j,i-1} - 2u_{j,i} + u_{j,i+1}}{h^2} + \gamma r_{j,i}\sqrt{\tau} \\ \text{and} \quad v_{j+1,i} &= v_{j,i} + \tau g_{j,i} + \tau D_v \frac{v_{j,i-1} - 2v_{j,i} + v_{j,i+1}}{h^2} + \gamma q_{j,i}\sqrt{\tau}, \end{aligned}\right\} \tag{3.2}$$

where noise is simulated with two uncorrelated random variables $r_{j,i}$ and $q_{j,i}$ distributed normally with the following parameters $\langle r_{j,i}\rangle = \langle q_{j,i}\rangle = 0$, $\langle r_{j,i}r_{k,l}\rangle = \langle q_{j,i}q_{k,l}\rangle = \delta_{j,k}\delta_{i,l}$, $\delta_{j,k} = 1$ if $j = k$ and $\delta_{j,k} = 0$ otherwise.

First, we consider the stochastic phenomenon known as noise-induced transitions between pattern-attractors in the Turing instability zone. Figure 6 shows the example of this process. At the beginning of the simulation, the stable (10 ↓) pattern is generated in the system in the absence of random perturbations. This state is used as the initial condition for the stochastic model. This structure is also preserved in the stochastic system (3.1) until $t \approx 300$, but after that, the (10 ↓) pattern is transformed by noise into the (9 ↓) pattern.

It should be noted that the stochastic transition from one spatial attractor to another can be explained by a different degree of sensitivity to noise of these coexisting attractors. While some patterns appear to be relatively stable, the others dissipate under the influence of random perturbations of increasing intensity. This indicates the constructive role of noise in the establishment of the more persistent attractor-pattern.

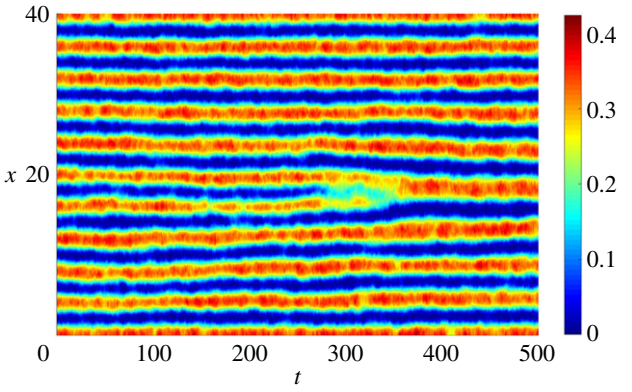

Figure 6. Noise-induced transition from (10 ↓) to (9 ↓) in the system (3.1) with $s = 1.2$, $c = 1$, $D = 0.05$ and $\gamma = 0.02$. (Online version in colour.)

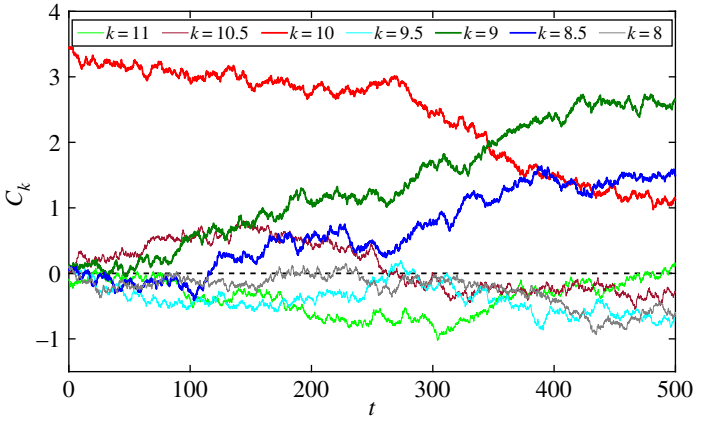

Figure 7. Temporal dynamics of modality coefficients of the stochastic system (3.1) with $s = 1.2$, $c = 1$, $D = 0.05$ and $\gamma = 0.02$ in the noise-induced transition from (10↓) to (9↓) pattern. (Online version in colour.)

The transition process can also be illustrated in terms of the modality analysis. Figure 7 illustrates the evolution of C_k over time for the process shown in figure 6. At the beginning of the simulation, the dominance of C_{10} is evident, while other modality coefficients are rather small. As the experiment progresses, the values of C_9 and $C_{8.5}$ increase, whereas C_{10} decays. For $t \approx 350$, the coefficient C_9 becomes dominant which reflects the changes shown in figure 6.

Consider now another important stochastic phenomenon of the noise-induced pattern formation. In the following example, we assume $s = 1.2$, $c = 1$ and $D = 0.15$. Note that the Turing bifurcation value is $D^* = 0.125$, so the deterministic distributed system belongs to the Turing stability zone, where the homogeneous equilibrium is stable and the pattern formation is impossible. However, we can show that even weak noise can generate non-homogeneous structures. Figure 8 displays the example of such a process. The noise intensity in this case is $\gamma = 0.02$, and the homogeneous equilibrium is used as the initial state of the model.

As can be seen from figure 8, random noise leads to the formation of a (5↑) pattern. This demonstrates the constructive role of random perturbations in self-organization processes. Figure 9 shows that the structure formed during this process is similar to the wave-like patterns which appear in the deterministic system in the zone of Turing instability.

This process can be further analysed with the help of modality coefficients C_k. The results of this analysis are shown in figure 10. The dynamics of modality coefficients is associated with the transient process and indeed demonstrates the final dominance of C_5.

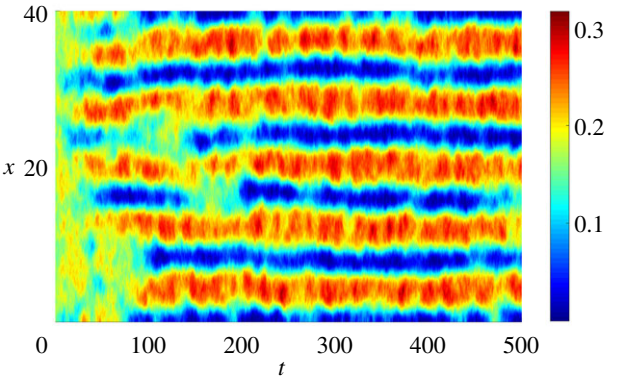

Figure 8. Noise-induced pattern formation in the system (3.1) with $s = 1.2$, $c = 1$, $D = 0.15$ and $\gamma = 0.02$. (Online version in colour.)

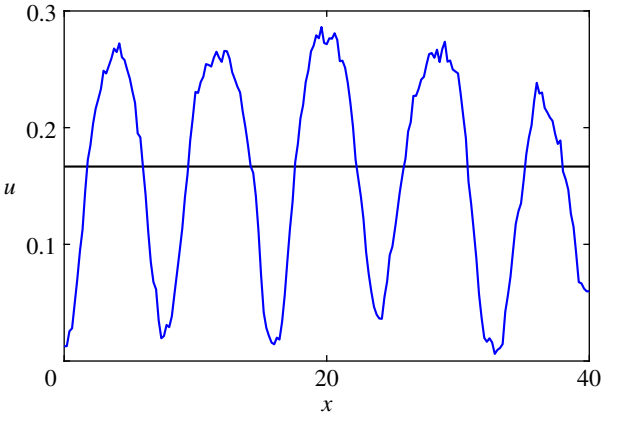

Figure 9. Noise-induced pattern formation for $s = 1.2$, $c = 1$, $D = 0.15$ and $\gamma = 0.02$. The snapshot is made at $t = 300$. (Online version in colour.)

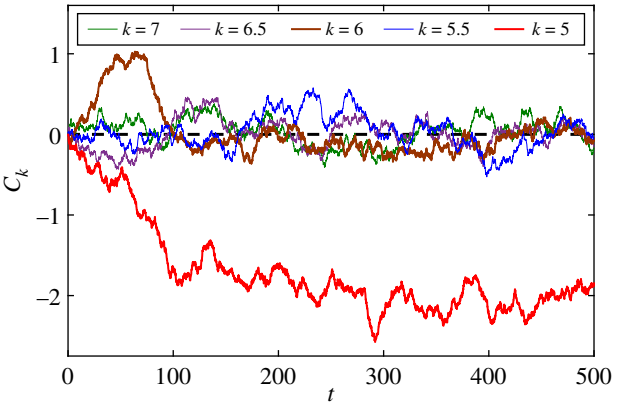

Figure 10. Temporal dynamics of modality coefficients of the stochastic system (3.1) with $s = 1.2$, $c = 1$, $D = 0.15$ and $\gamma = 0.02$. (Online version in colour.)

Despite the constructive role of noise, it can also be destructive. It is clear that noise with higher intensity will not cause pattern formation; instead, it will confusedly mix possible patterns of the system. It is assumed that the noise-induced formation of a dominant pattern is only possible

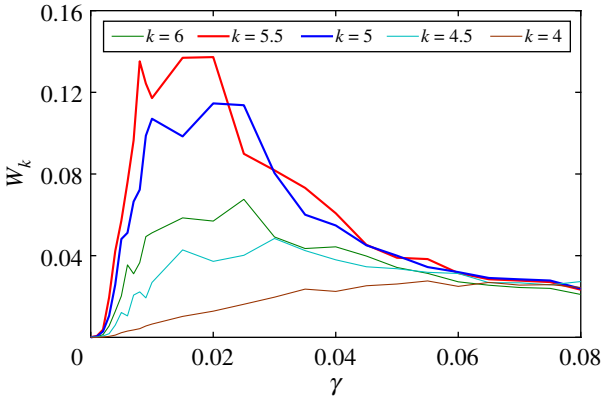

Figure 11. Noise-induced pattern formation for $s = 1.2$, $c = 1$ and $D = 0.13$. Average modality powers versus noise intensity. (Online version in colour.)

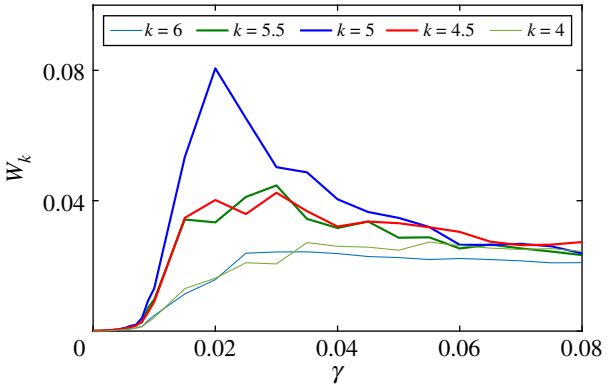

Figure 12. Noise-induced pattern formation for $s = 1.2$, $c = 1$ and $D = 0.15$. Average modality powers versus noise intensity. (Online version in colour.)

when the noise intensity takes values within a particular range. Outside this interval, noise is either too weak to disturb the homogeneous state or too strong to preserve a specific structure.

In order to detect the appearance of a stable pattern, the modality analysis is used along with modality power coefficients defined as

$$W_k = \left\langle \frac{1}{T} \int_0^T C_k{}^2(t)\, \mathrm{d}t \right\rangle. \tag{3.3}$$

Larger values of W_k imply that the corresponding pattern dominates in the modelling process. Due to the stochastic nature of the obtained results, the statistical analysis is applied. For each value of the noise intensity, the calculations are repeated 100 times and the modality power coefficients are averaged. The averaged W_k are shown in figures 11 and 12 for $D = 0.13$ and $D = 0.15$, respectively.

The values of W_5 and $W_{5.5}$ in figure 11 (for $D = 0.13$) sharply rise over other values within $\gamma \in [0, 0.04]$. In this interval, the structures similar to the 5-peak and 5.5-peak patterns can be expected. A further increase in the noise intensity γ makes all modes equally prominent, which in turn results in an unstable and unpredictable behaviour.

Consider now figure 12 for $D = 0.15$, where in the interval $\gamma \in [0, 0.04]$ one can see the dominance of W_5 only, which describes the 5-peak pattern power. This dominance is the most

evident near $\gamma = 0.02$. This result is in good agreement with details shown in figures 8–10. A further increase in the noise intensity results in the mixing of all modes. So, the stochastic generation of the evident spatial structures only occurs for some 'optimal' value of the noise intensity. This phenomenon can be interpreted as a kind of stochastic resonance in distributed systems.

4. Conclusion

In this paper, we have demonstrated several phenomena of the nonlinear predator–prey model with diffusion. We have shown that the deterministic system can exhibit a multistable behaviour when coexisting stable spatially heterogeneous patterns are generated in the Turing instability zone. Because of this multistability, noise-induced transitions between the coexisting spatial attractors-patterns are possible. Additionally, we have demonstrated how random perturbations can generate heterogeneous patterns in the Turing stability zone. We have applied the modality analysis for a quantitative description of the processes of the patterns generation and transformation. This method allows one to reveal some kind of stochastic resonance; some modes are significantly amplified by random noise of a certain intensity. We believe that our approach is readily applicable to the study of similar phenomena in more complex models.

Data accessibility. This article has no additional data.

Authors' contributions. All authors contributed equally.

Competing interests. We declare we have no competing interests.

Funding. The work was supported by the Russian Science Foundation (grant no. 16-11-10098).

References

1. Cross M, Greenside H. 2009 *Pattern formation and dynamics in nonequilibrium systems*. Cambridge, UK: Cambridge University Press.
2. D'Odorico P, Laio F, Ridolfi L. 2006 Vegetation patterns induced by random climate fluctuations. *Geophys. Res. Lett.* **33**, L19404. (doi:10.1029/2006GL027499)
3. Gambino G, Lombardo MC, Sammartino M, Sciacca V. 2013 Turing pattern formation in the Brusselator system with nonlinear diffusion. *Phys. Rev. E* **88**, 042925. (doi:10.1103/PhysRevE.88.042925)
4. Smith-Roberge J, Iron D, Kolokolnikov T. 2019 Pattern formation in bacterial colonies with density-dependent diffusion. *Eur. J. Appl. Math.* **30**, 196–218. (doi:10.1017/S0956792518000013)
5. Zhou J, Shi J. 2015 Pattern formation in a general glycolysis reaction-diffusion system. *IMA J. Appl. Math.* **80**, 1703–1738. (doi:10.1093/imamat/hxv013)
6. Alqahtani AM. 2018 Numerical simulation to study the pattern formation of reaction-diffusion Brusselator model arising in triple collision and enzymatic. *J. Math. Chem.* **56**, 1543–1566. (doi:10.1007/s10910-018-0859-8)
7. Hoyle R. 2006 *Pattern formation: an introduction to methods*. Cambridge, UK: Cambridge University Press.
8. Morton KW. 2005 *Numerical solution of partial differential equations: an introduction*. Cambridge, UK: Cambridge University Press.
9. Turing AM. 1952 The chemical basis of morphogenesis. *Phil. Trans. R. Soc. Lond. B* **237**, 37–72. (doi:10.1098/rstb.1952.0012)
10. Nicolis G, Prigogine I. 1977 *Self-organization in nonequilibrium systems*. New York, NY: Wiley.
11. Sander E, Wanner T. 2003 Pattern formation in a nonlinear model for animal coats. *J. Differ. Equ.* **131**, 143–174. (doi:10.1016/S0022-0396(02)00156-0)
12. Fiasconaro A, Valenti D, Spagnolo B. 2004 Nonmonotonic behavior of spatiotemporal pattern formation in a noisy Lotka–Volterra system. *Acta Phys. Pol. B* **35**, 1491–1500.
13. Valenti D, Fiasconaro A, Spagnolo B. 2004 Pattern formation and spatial correlation induced by the noise in two competing species. *Acta Phys. Pol. B* **35**, 1481–1489.
14. Wang X, Lutscher F. 2019 Turing patterns in a predator-prey model with seasonality. *J. Math. Biol.* **78**, 711–737. (doi:10.1007/s00285-018-1289-8)

15. Zhao H, Huang X, Zhang X. 2014 Turing instability and pattern formation of neural networks with reaction-diffusion terms. *Nonlinear Dyn.* **76**, 115–124. (doi:10.1007/s11071-013-1114-2)
16. Baurmann M, Gross T, Feudel U. 2007 Instabilities in spatially extended predator-prey systems: spatio-temporal patterns in the neighborhood of Turing–Hopf bifurcations. *J. Theor. Biol.* **245**, 220–229. (doi:10.1016/j.jtbi.2006.09.036)
17. Ledesma-Duran A, Aragon JL. 2019 Spatio-temporal secondary instabilities near the Turing-Hopf bifurcation. *Sci. Rep.* **9**, 11287. (doi:10.1038/s41598-019-47584-9)
18. Meixner M, De Wit A, Bose S, Scholl E. 1997 Generic spatiotemporal dynamics near codimension-two Turing-Hopf bifurcations. *Phys. Rev. E* **55**, 6690. (doi:10.1103/PhysRevE.55.6690)
19. Ricardo M, Mishler S. 2009 Turing instabilities at Hopf bifurcation. *J. Nonlinear Sci.* **19**, 467–496. (doi:10.1007/s00332-009-9041-6)
20. Anishchenko V, Astakhov V, Neiman A, Vadivasova T, Schimansky-Geier L. 1988 *Nonlinear dynamics of chaotic and stochastic systems. Tutorial and modern development*. Berlin, Germany: Springer.
21. Bashkirtseva I, Ryashko L. 2002 Sensitivity analysis of stochastically forced Lorenz model cycles under period doubling bifurcations. *Dyn. Syst. Appl.* **11**, 293–310.
22. McDonnell M, Stocks N, Pearce C, Abbott D. 2008 *Stochastic resonance: from suprathreshold stochastic resonance to stochastic signal quantization*. Cambridge, UK: Cambridge University Press.
23. Fedotov S, Iomin A, Ryashko L. 2011 Non-Markovian models for migration-proliferation dichotomy of cancer cells: anomalous switching and spreading rate. *Phys. Rev. E* **84**, 061131. (doi:10.1103/PhysRevE.84.061131)
24. Bashkirtseva I, Neiman AB, Ryashko L. 2015 Stochastic sensitivity analysis of noise-induced suppression of firing and giant variability of spiking in a Hodgkin-Huxley neuron model. *Phys. Rev. E* **91**, 052920. (doi:10.1103/PhysRevE.91.052920)
25. Horsthemke W, Lefever R. 1984 *Noise-induced transitions*. Berlin, Germany: Springer.
26. Gao J, Hwang S, Liu J. 1999 When can noise induce chaos? *Phys. Rev. Lett.* **82**, 1132–1135. (doi:10.1103/PhysRevLett.82.1132)
27. Pisarchik A, Feudel U. 2014 Control of multistability. *Phys. Rep.* **540**, 167–218. (doi:10.1016/j.physrep.2014.02.007)
28. Bashkirtseva I, Ryashko L, Stikhin P. 2013 Noise-induced chaos and backward stochastic bifurcations in the Lorenz model. *Int. J. Bifurcation Chaos* **23**, 1350092. (doi:10.1142/S0218127413500922)
29. Bashkirtseva I, Ryashko L. 2018 Noise-induced shifts in the population model with a weak Allee effect. *Physica A* **491**, 28–36. (doi:10.1016/j.physa.2017.08.157)
30. Dobramysl U, Mobilia M, Pleimling M, Tauber U. 2018 Stochastic population dynamics in spatially extended predator-prey systems. *J. Phys. A: Math. Theor.* **51**, 063001. (doi:10.1088/1751-8121/aa95c7)
31. Bashkirtseva I, Pankratov A. 2019 Stochastic Higgins model with diffusion: pattern formation, multistability and noise-induced preference. *Eur. Phys. J. B* **92**, 238. (doi:10.1140/epjb/e2019-100291-4)
32. Dangelmayr G, Oprea I. 2004 *Dynamics and bifurcation of patterns in dissipative systems*. Singapore: World Scientific.
33. Liu X, Zhang T, Meng X, Zhang T. 2018 Turing-Hopf bifurcations in a predator-prey model with herd behavior, quadratic mortality and prey-taxis. *Physica A* **496**, 446–460. (doi:10.1016/j.physa.2018.01.006)
34. Yuan S, Xu C, Zhang T. 2013 Spatial dynamics in a predator-prey model with herd behavior. *Chaos* **23**, 033102. (doi:10.1063/1.4812724)